ARMY RESEARCH LABORATORY

Silicon Carbide Photoconductive Switches

by Stephen E. Saddow

ARL-TR-388

September 1994

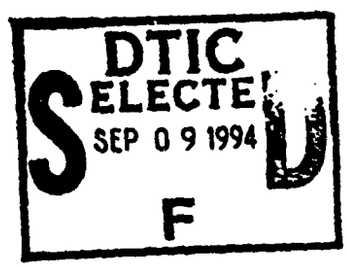

The findings in this report are not to be construed as an official Department of the Army position unless so designated by other authorized documents.

Citation of manufacturer's or trade names does not constitute an official endorsement or approval of the use thereof.

Destroy this report when it is no longer needed. Do not return it to the originator.

REPORT DOCUMENTATION PAGE

Form Approved
OMB No. 0704-0188

1. AGENCY USE ONLY (Leave blank)	2. REPORT DATE	3. REPORT TYPE AND DATES COVERED
	September 1994	Final, October 1992–December 1993

4. TITLE AND SUBTITLE
Silicon Carbide Photoconductive Switches

5. FUNDING NUMBERS
PE: 61102

6. AUTHOR(S)
Stephen E. Saddow

7. PERFORMING ORGANIZATION NAME(S) AND ADDRESS(ES)
U.S. Army Research Laboratory
Attn: AMSRL-WT-NF
2800 Powder Mill Road
Adelphi, MD 20783-1197

8. PERFORMING ORGANIZATION REPORT NUMBER
ARL-TR-388

9. SPONSORING/MONITORING AGENCY NAME(S) AND ADDRESS(ES)
U.S. Army Research Laboratory
Attn: AMSRL-WT-NA
2800 Powder Mill Road
Adelphi, MD 20783-1197

10. SPONSORING/MONITORING AGENCY REPORT NUMBER

11. SUPPLEMENTARY NOTES
AMS code: 611102.H440011
ARL PR: 4AE125

12a. DISTRIBUTION/AVAILABILITY STATEMENT
Approved for public release; distribution unlimited.

12b. DISTRIBUTION CODE

13. ABSTRACT (Maximum 200 words)

The optoelectronic properties of *p*-type 6-H silicon carbide (6H-SiC) have been investigated in an experiment that used lateral and vertical photoconductive (PC) switches. Both photovoltaic and photoconductive effects are reported, which were observed on switches using both geometries and measured at several wavelengths near the 6H-SiC absorption edge. PC techniques were employed to measure the surface and bulk carrier lifetimes of 40 and 200 ns, respectively. The switches displayed a high-speed photovoltaic response to picosecond laser excitations in the UV and visible spectral regions. In particular, efficient subnanosecond optical absorption processes were observed in the visible region.

The photovoltage was measured as a function of both laser wavelength (and hence absorption depth) and laser beam position within the switching gap. The switch response to picosecond laser pulses in the UV, violet, green, and red spectral regions was shown to have subnanosecond photovoltaic response times. Finally, since the optical absorption coefficient had not been well established for device-grade 6H-SiC, the optical absorption coefficient near the 6H-SiC bandgap energy (E_g) was also measured, and the bandgap was determined to be approximately 3.1 eV.

14. SUBJECT TERMS	15. NUMBER OF PAGES
6H-SiC, photoconductive, photovoltaic, absorption coefficient, switch, silicon carbide	27
	16. PRICE CODE

17. SECURITY CLASSIFICATION OF REPORT	18. SECURITY CLASSIFICATION OF THIS PAGE	19. SECURITY CLASSIFICATION OF ABSTRACT	20. LIMITATION OF ABSTRACT
Unclassified	Unclassified	Unclassified	SAR

Contents

Figures

Table

1. Introduction

Silicon carbide (SiC) is potentially suitable for high-speed and high-power photoconductive (PC) switching applications since it is a semiconductor material with a wide band-gap energy of ~3 eV. As such, SiC is suitable for two applications where gallium arsenide and silicon cannot compete—high temperature and high power. Because of the material's large thermal conductivity and high breakdown electric field, which are both approximately 10 times greater than those of GaAs, SiC may be ideally suited for optoelectronic applications. It was with this in mind that my colleagues and I conducted extensive research to determine the feasibility of using the 6H silicon-carbide (6H-SiC) polyphase for PC switching applications.

Although the optoelectronic potential of SiC has been known since 1907 [1], only recently has electronic device grade SiC been available [2]. In this report I describe how the optoelectronic properties of 6H-SiC were investigated with lateral and vertical photoconductive switches. I report the measurement of photovoltaic and photoconductive effects for both geometries and at several wavelengths near the 6H-SiC absorption edge. The PC carrier lifetime in *p*-type 6H-SiC was measured, with surface and bulk PC carrier lifetimes determined to be 40 and 200 ns, respectively [3]. Although the devices possess dark resistances on the order of 10 Ω, the switching efficiency of the vertical switches approached 32 percent, while the resistance of the lateral devices could be reduced by 50 percent with 200 μJ of laser radiation at λ = 337 nm.

In addition, I measured photoconductivity in the vertical switches with a device static power dissipation exceeding 11 W. Although the semiconductor glowed from the high level of dc power being dissipated, only the switch mount was damaged. This is further proof that 6H-SiC is indeed a high-temperature optoelectronic material.

Section 2 presents the results of a detailed study of the photovoltaic (PV) properties of 6H-SiC. The photovoltaic response was measured as a function of laser-beam position and laser wavelength (near the 6H-SiC absorption edge). A nitrogen laser with a 7-ns pulse width was used to measure an efficient PV effect (I generated a 40-mV signal using a 200-μJ pulse at 337 nm). In addition, this material displayed a high-speed PV response to picosecond laser excitations; measurement-limited subnanosecond PV response times were observed for laser photon energies less than the 6H-SiC band gap energy. The photovoltaic response was measured as a function of laser wavelength and beam spatial position within the switching

gap, along with the PC carrier lifetime and optical absorption coefficient. The data show that the measured photovoltage is a sensitive function of both spatial position and optical absorption depth. Hypothetical arguments are presented that qualitatively explain the observed PV effects.

The switch response to picosecond laser pulses in the UV, violet, green, and red spectral regions are shown to have subnanosecond photovoltaic response times. Finally, since the optical absorption coefficient has not been well established for device-grade 6H-SiC, the optical absorption coefficient near the 6H-SiC band-gap energy ($E_g \sim 3$ eV) was also measured. For these samples the measured value of E_g was approximately 3.1 eV.

The PC measurements were made on switches of both device geometries placed in a low-impedance dc circuit, which was designed for maximum sensitivity. These measurements are described in section 4. In a setup using lateral PC switches and above-band-gap radiation, the PC carrier lifetime at the SiC crystal surface was measured and found to be approximately 40 ns. In a setup using vertical switches and below-band-gap radiation, the bulk SiC PC carrier lifetime was determined to be approximately 200 ns for this material. In both cases, the PC response showed a double-exponential decay, with both a fast component and a slower component, which I attribute to direct electron-hole recombination and re-emission of trapped charge, respectively. This same behavior was observed by Okumura et al [4] in 3C-SiC.

The primary technological barrier to the use of SiC as a PC switch material is the low substrate and epitaxial layer resistivity values attainable to date. Using deep-level transient spectroscopy (DLTS) and *p-n* junction diodes provided by NASA Lewis Research Center, my colleagues and I made measurements at Old Dominion University in an attempt to identify both shallow and deep-level electronic impurities in 6H-SiC. To date, we have identified what we believe to be a fairly deep-level impurity with an activation energy of 0.58 eV. This is the subject of a separate report [5].

Although 6H-SiC is a relatively new material as far as electronic-grade substrates are concerned, considerable research into the material constants and growth of SiC substrates and epitaxial films has been reported in the literature [6–9]. In particular, invited review articles by Davis et al [10] and Trew et al [11] discuss most of the relevant issues relating to this new and exciting semiconductor material.

Because of this extensive coverage in the literature, I do not dwell on the numerous materials issues, but rather simply compare the relevant properties of SiC with those of GaAs and Si, and point out the important differences. Table 1 compares the relevant material properties of Si, GaAs, and 6H-SiC.

The most important material properties of SiC, GaAs, and Si for the optoelectronic attenuator application are the electron and hole mobilities and saturated drift velocity. Table 1 shows that 6H-SiC has lower carrier mobility than Si or GaAs but a higher saturated drift velocity, which would normally be a disadvantage for any semiconductor material. However, since the maximum operating electric field for 6H-SiC is approximately 10 times greater than for GaAs, the lower mobility values are offset by the higher saturated velocity.

As far as thermal behavior is concerned, clearly 6H-SiC is superior to both GaAs and Si, with a thermal conductivity more than 3.3 times that of Si and 10 times that of GaAs. This point is also evident from the greatly increased maximum operating temperature of 6H-SiC. Thus, for high-power and ultra-fast applications where high-electric-field regions are present in PC switches, 6H-SiC has an obvious advantage over both Si and GaAs. It was with these points in mind that I set out to explore the suitability of 6H-SiC as a high-speed and high-power PC switching material.

Table 1. Comparison of properties of SiC, Si, and GaAs.

Property	Si	GaAs	6H-SiC
Band-gap energy (eV)	1.1	1.4	3.0
Maximum operating temperature (K)	600	760	1580
Melting point (K)	1690	1510	2100*
Band-gap type	Indirect	Direct	Indirect
Electron mobility ($cm^2/V\text{-}s$)	1400	8800	400
Hole mobility ($cm^2/V\text{-}s$)	600	400	40
Breakdown field (10^5 V/cm)	3	4	40–60
Thermal conductivity (W/cm-K)	1.5	0.5	5
Saturated electron drift velocity (10^7 cm/s)	1	2	2.5
Dielectric constant	11.8	12.8	10.0

*Sublimation occurs at this temperature.

2. SiC Photoconductive Switch Design and Fabrication

P-type 6H-SiC substrates were selected for this investigation. These substrates were not semi-insulating, since the bulk resistivity was only 0.5 Ω-cm. This presents a serious problem for PC switching because of the low value of dark resistance. As a way to circumvent this problem, high-resistivity (22 Ω-cm) *p*-doped epi-layers were grown on a 1-in. wafer (see fig. 1).* The epi-layer thickness was 20 μm. A highly doped p^{++} ($N_A > 10^{19}$ cm^{-3}) layer was then grown on top of the *p* epi-layer to achieve ohmic contact to the material. The p^{++} epi-layer was then reactive ion etched [12] in NF_3 (with Al used as the etchant mask) so that the simple gap of the lateral switch could be electrically isolated. Al-Ti alloy contacts [13] were then formed on top of the p^{++} mesas with a smaller (10-μm undersized) contact pattern. After the ohmic contacts were annealed, gold overlayers were deposited on top and patterned with the same mask. Current-voltage (*I-V*) measurements made on a curve tracer displayed ohmic contact behavior. The lateral switch dark resistance varied from 13 to 20 Ω across the wafer.

The lateral device contact geometry used was a microstrip line with a simple gap *L* of 10 μm, 0.5 mm, or 3 mm, as shown in figure 1. A ground plane was deposited to form a 50-Ω characteristic impedance; however, this contact was not connected to circuit ground during these experiments, since the device was placed on a piece of Mylar film. This was done so that the photocarriers would flow between the two microstrip contacts and not be shunted to ground by the low-impedance substrate. The microstrip line width was 465 μm.

For the vertical PC switches, a 170-Ω-cm epitaxial layer was grown on the SiC substrate (see fig. 2). The epi-layer thickness was 20 μm. Highly doped p^{++} ($N_A > 10^{19}$ cm^{-3}) layers were then grown on top of these epi-layers to achieve ohmic contact to the material. Al/Ti alloy contacts were then patterned in identical fashion as the lateral switches, except for the contact geometry. The contacts consisted of

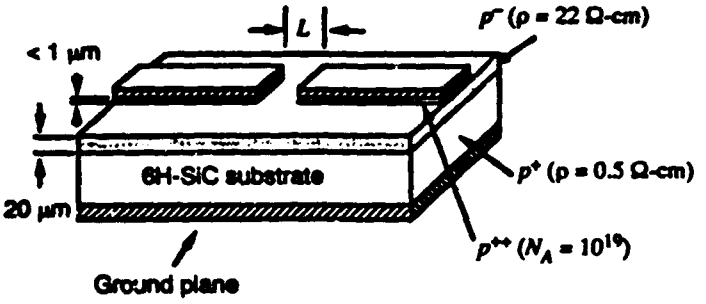

Figure 1. Schematic view of lateral PC switch design with simple switching gap of length *L*. Overall device length is 1 cm.

*Cree Research, Inc., 2810 Meridian Parkway, Suite 176, Durham, NC 27713.

a gridded top electrode with a solid bottom electrode (fig. 2). The gridded top electrode was designed for maximum optical coupling efficiency, which implies a metal-to-open-area ratio of 1:1. The solid bottom electrode was recessed from the SiC chip edges to reduce leakage currents. Although only the top electrode was fabricated on a highly doped (p^{++}) epi-layer, the low substrate resistivity yielded ohmic contact, as indicated by *I-V* measurements on a Tektronix 576 curve tracer. The dark resistance varied from 8 to 10 Ω for the vertical devices.

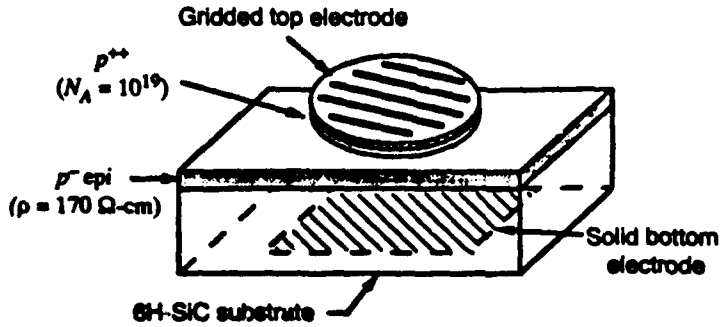

Figure 2. Schematic view of vertical PC switch design showing gridded top electrode. Solid bottom electrode was placed at center of device to suppress leakage currents on chip edges. Device size 1 × 1 cm.

3. Photovoltaic Experiments Using Lateral Switches

Various measurements were performed in the assessment of the PV response of 6H-SiC. Both "near-band-gap" and "high-speed" picosecond measurements were performed with two different UV laser systems (sect. 3.1 and 3.2). Section 3.3 discusses the PV data and the rather unusual observed PV response. Since time did not permit experimental verification of the analysis that is presented, it is only of a qualitative nature, intended to form the basis of a more detailed analysis planned for the future.

3.1 Near-Band-Gap Measurements

The experimental setup used to determine the PV response near the 6H-SiC band-gap energy is shown in figure 3. A UV/violet dye (Exciton, Inc., No. PBBO) was pumped with an XeCl excimer laser so that the laser wavelength could be tuned through the 6H-SiC absorption edge (385 nm $\leq \lambda_{dye} \leq$ 430 nm). For reference, the published band-gap energy of this material is 3 eV, which corresponds to a photon wavelength of 414 nm. I used the XeCl (λ = 308 nm) laser output to directly assess the switch behavior well above band gap. The XeCl laser output energy was ≈18 μJ, with a 15-ns pulse width and a 1-Hz repetition rate. The dye output energy was maintained at ≈16 ± 1.6 μJ, with a 5-ns pulse width and 1-Hz repetition rate. The dye wavelength could be measured to within 1 nm.

Figure 4 shows the measured PV response from a 10-μm-gap lateral PC switch when activated by the N_2 laser. A dependence of the PV response on the laser beam position was observed. Since the 1-mm spot size was much greater than the switch gap, the spot was positioned in one of three positions: covering the gap (position 2), or at the edge of one of the metalized microstrip lines (positions 1 and 3). Inspection of the data shows that the PV response of the 10-μm

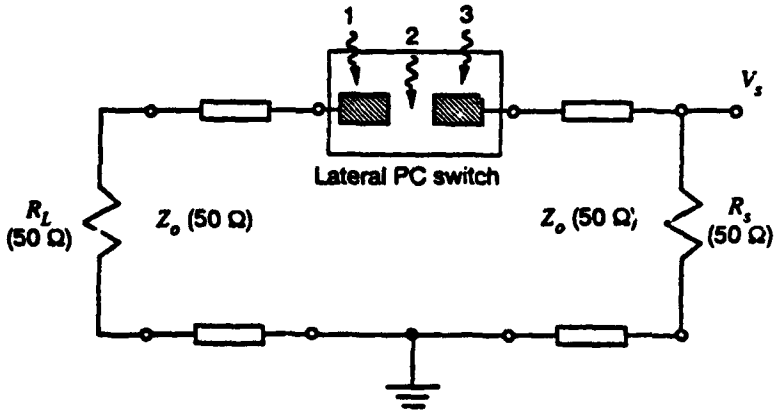

Figure 3. Symmetrical circuit used to measure 6H-SiC PV response. Laser spot size ≈1 mm. Beam positions 1, 2, and 3 correspond to measured values in figure 4. R_s and R_L are oscilloscope and matched loads, respectively. L ≈ 10 μm.

SiC PC switch is fairly fast; the PV decay time for positions 1 and 3 is approximately 10 ns, as indicated in the figure. These data suggest that 6H-SiC may be suitable for high-speed UV detection applications.

For a full understanding of this high-speed PV response, the spot size relationship with respect to the switching gap must be better controlled. Using the symmetrical circuit of figure 5, I illuminated a 3-mm-gap lateral PC switch with the XeCl laser directly (λ = 308 nm) to assess the above-band-gap (i.e., $h\nu_{laser} > E_g$) device performance. The laser spot size was on the order of 0.5 mm. A PV effect was observed with the polarity of the detected photovoltage being dependent on the laser beam position with respect to the switch gap and scope connection, as shown in figure 6. Note that the PV signal polarity for laser beam positions at X = 0 and 3 mm is reversed. When the positions of the matched 50-Ω cable and scope termination were reversed, the behavior observed was identical to that shown in the figure; thus, the switch behavior is symmetrical.

Also shown in figure 6 is the PV response as a function of laser position measured with below-band-gap radiation (λ = 431 nm). There are two major differences between these data and the 308-nm data:

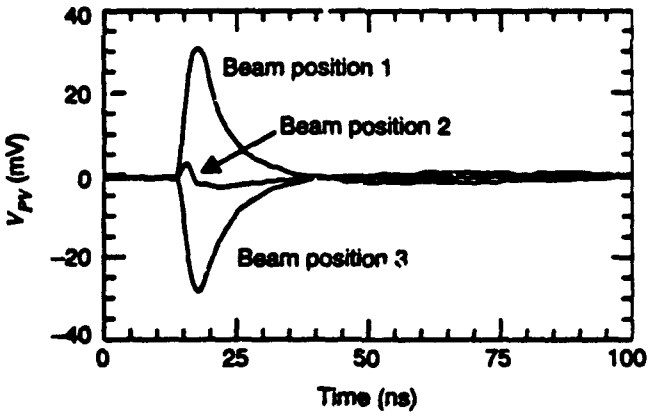

Figure 4. PV response of a 10-μm-gap lateral switch. Laser pulse width was 7.7 ns (λ = 337 nm). Pulse decay time ≈ 10 ns. Beam positions defined in figure 3.

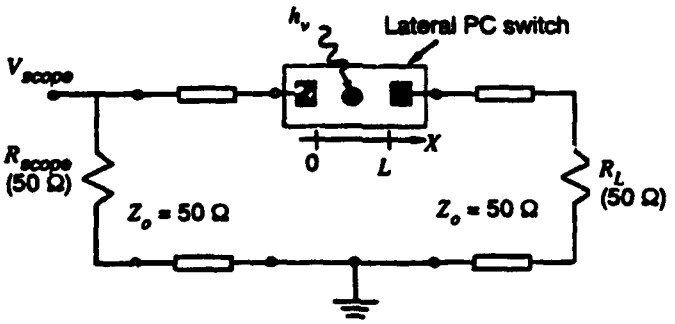

Figure 5. Symmetrical circuit configuration used to measure 6H-SiC PV response. Laser spot size ≤ 1 mm. X denotes beam position within gap.

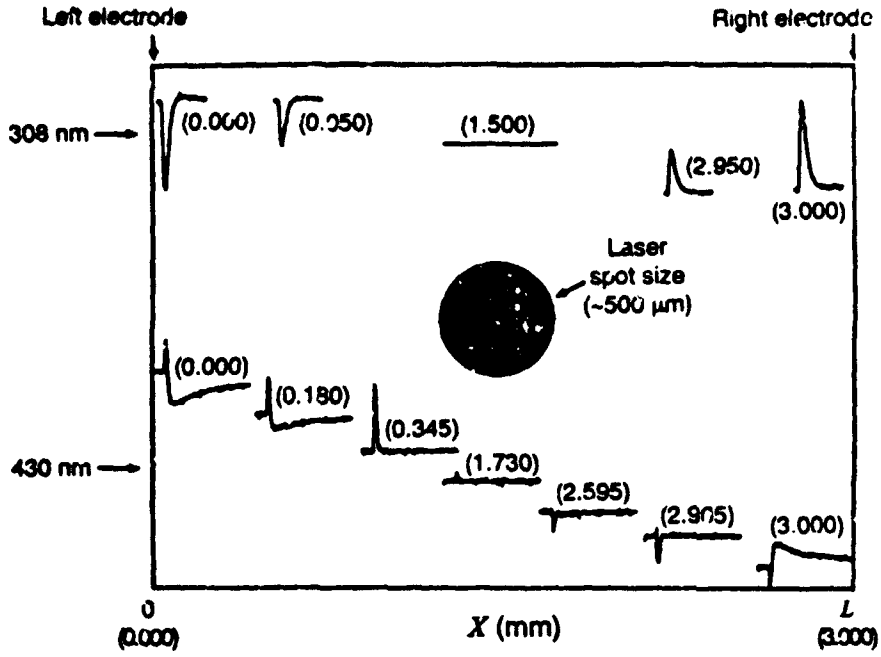

Figure 6. PV signal waveform dependence as a function of laser beam position. Responses at both 308 nm ($h\upsilon > E_g$) and 450 nm ($h\upsilon < E_g$) are shown. Laser beam position in switching gap indicated in parentheses.

First, the PV signal never reaches zero value anywhere within the switch gap. Second, the PV response contains more structure, with both positive- and negative-polarity signal components present. Some proposed explanations for these observations are discussed in section 3.3.

The peak photovoltage was measured as a function of laser wavelength and is shown in figure 7. Because of the low signal amplitude, 10 waveforms were measured, then averaged to complete this figure. The laser beam position was at X = 0.0 mm with a 0.5-mm spot size. The figure shows that the peak PV response occurs at about 401 nm, while the peak optical output of blue SiC light-emitting diodes (LED's) occurs at approximately 472 nm [14]. This apparent difference between the peak PV response and the peak spectral output of blue LED's may be due to the different material structures used to fabricate the respective devices: p-n junction diodes for blue LED's, and p-p^+ junctions here for the lateral and vertical PC switches. In addition, $\lambda_{absorption\ coef} < \lambda_{emission}$ is typically observed with LED's, with which these results are consistent.

The optical absorption coefficient, α, of p-type 6H-SiC was also measured (see fig. 8) with the XeCl/dye laser system via an optical transmission measurement. The absorption coefficient was calculated assuming a refractive index of 2.58. Note that α depends strongly on λ, and thus on the absorption depth. This indicates that carrier generation for photon energies above and below E_g may

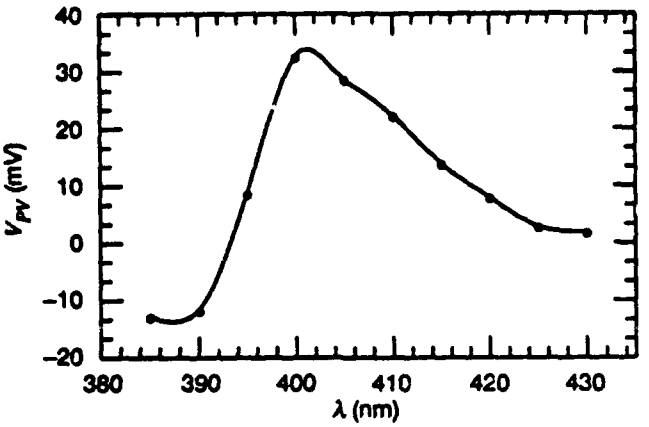

Figure 7. Average peak PV response of lateral device versus λ. Laser beam position: X = 0.0 mm. Note: Peak PV response at 401 nm.

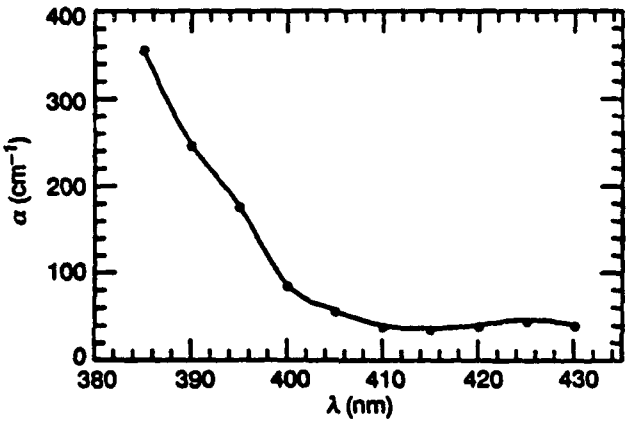

Figure 8. Measured optical absorption coefficient, α, as a function of photon energy. Measurements made with XeCl-pumped UV/violet PBBO dye.

occur in different epi-layer regions of the device, because of changes in the optical penetration depths at these different wavelengths. As a result, there should be a positional dependence of the PV response at wavelengths above and below E_g due to the device structure, and figure 6 appears to support this conclusion. Section 3.3 gives further details of how all the SiC PV response data can be used to draw conclusions pertaining to device performance.

3.2 High-Speed Picosecond Measurements

The high-speed PV measurements were made on a 3-mm-gap lateral PC switch under the same setup as figure 5, except that a picosecond laser system was used in place of the XeCl/dye laser system [15]. Several picosecond measurements were made at the following wavelength regimes: UV (λ = 266 nm), violet (λ = 450 nm), green (λ = 532 nm), and red (λ = 705 nm). The laser pulse widths for the UV, green, and red wavelengths were ~10 ps, with the green pulse width being ~150 ps. The energies were ~10, 20, 200, and 40 μJ for the UV,

violet, green, and red wavelengths, respectively. The laser spot was centered at X = 0.0 mm (spot size for all cases ≤1.5 mm). Figure 9 shows the resulting PV response for these picosecond laser excitations.

The observed photovoltage under violet (λ = 450 nm) excitation is shown in figure 9(b). Note that there is a subnanosecond PV rise time followed by two distinct decay times: a fast subnanosecond decay time followed by a slower 4-ns decay time. For photon ener-

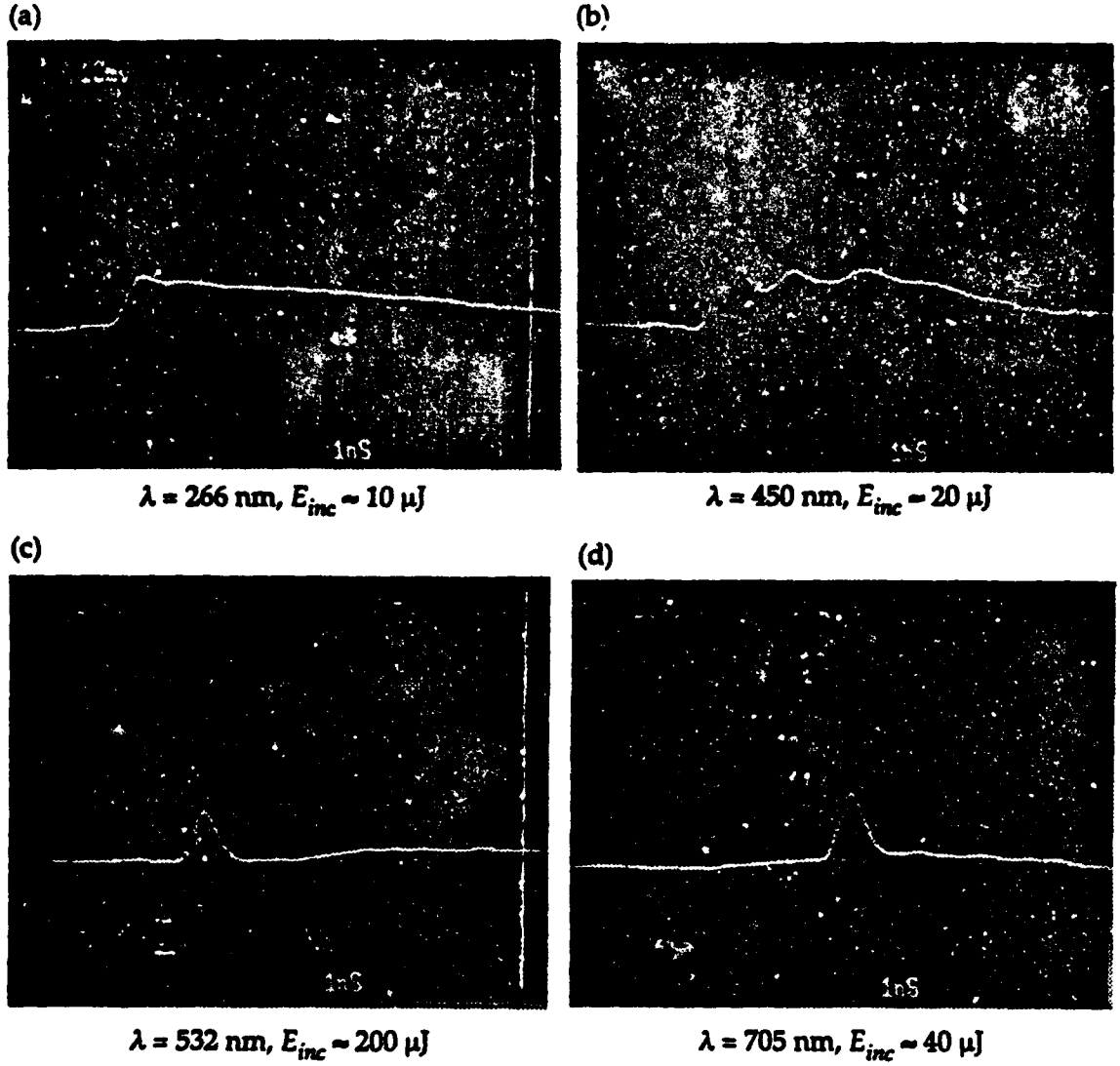

Figure 9. Picosecond PV response of a 3-mm-gap lateral 6H-SiC PC switch: (a) UV PV response, oscilloscope-limited rise time, 6-ns fall time, (b) visible (violet) PV response, oscilloscope-limited rise time, and initial fall time, (c) visible (green) PV response, oscilloscope-limited rise and fall times, and (d) visible (red) PV response, oscilloscope-limited rise and fall times. Beam position (fig. 6): X = 0.

gies well below E_g (i.e., for the green, fig. 9(c), and red, fig. 9(d), laser excitations), the PV response rise time was identical, while only the subnanosecond fall time was observed. It should be noted that these measurements were limited by the 1-GHz bandwidth of the analog oscilloscope. When the photon energy was greater than E_g (i.e., during UV excitation), the response had the same subnanosecond rise time, but only the slow decay time was observed, which was ≈6 ns.

3.3 Photovoltaic Experimental Discussion

The successful measurement of a significant high-speed PV effect in 6H-SiC indicates that efficient UV photodetection at high temperatures is possible [16]. The very fast carrier decay times ($\tau_{decay} \leq 1$ ns for below-band-gap radiation) observed during these experiments indicate that the UV detection is also high speed. The central question therefore is, what are the mechanisms responsible for the observed variation in photovoltage as a function of laser wavelength and beam position? For insight, I offer the following qualitative arguments. These arguments must show a correlation between the dependence of the PV response on carrier generation, both in terms of the spatial position of the laser beam within the gap and in terms of the optical absorption depth of the laser photons within the semiconductor. Therefore, any model of the PV response must show qualitative agreement between the material structure and the device geometry.

Figure 10, a scanning electron microscope (SEM) image of the contact region, shows that the p^{++} epi-layer protrudes ≈5 μm from the Al-Ti alloy contact edge. Figure 11 shows the proposed energy band

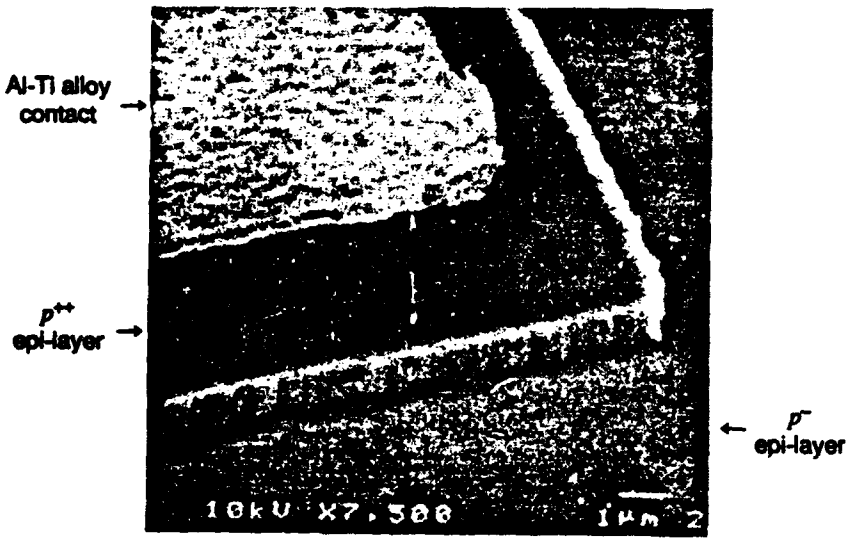

Figure 10. SEM image of metal/semiconductor interface showing a 5-μm p^{++} epi-layer protrusion.

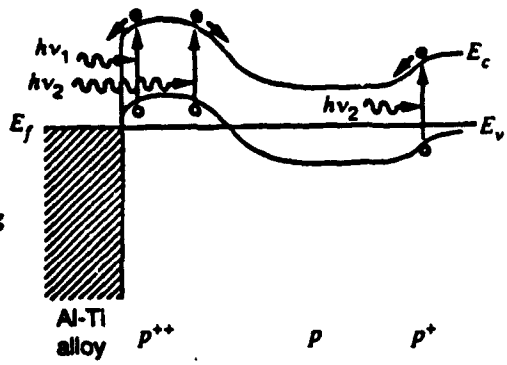

Figure 11. Proposed energy band diagram for contact region shown in figure 10. Photon energies above and below E_g are indicated by $h\nu_1$ and $h\nu_2$, respectively, along with corresponding electron drift directions.

diagram for the lateral devices. Upon illumination of this region with above-band-gap radiation, designated by $h\nu_1$ in figure 11, carriers are generated near the Al-Ti alloy/p^{++} interface. This metal/semiconductor interface is modeled as a Schottky contact. Although curve tracer data show ohmic-like contact behavior, the junction behavior in the presence of optically injected electrons results in a Schottky contact region (also, the *I-V* measurements are dominated by the low-resistivity substrate, not the p^{++} epi-layer; this also makes the contact look "ohmic like"). Therefore, carriers generated at this junction will be separated by the built-in Schottky potential, with electrons entering the metal and holes being swept into the bulk. Measurement of a voltage pulse with a negative polarity (see fig. 6, 308 nm, X = 0.0 mm) supports this hypothesis.

The polarity of the measured photovoltage is a function of where one measures the PV with respect to the position of the laser spot, as the data in figures 4 and 6 indicate. This can be explained by a simple charge neutrality argument, whereby if one assumes that the switch gap must remain electrically neutral, then any charge that is swept out of the switch gap and into the metal must be compensated by the same polarity charge being injected at the other contact. If a negative voltage pulse is measured at the left (i.e., oscilloscope) contact, this implies that a positive pulse should be measured at the other contact, since this contact must inject electrons for the device to remain neutral; therefore, a net positive charge is detected at that contact during electron injection. Careful inspection of figures 4 and 6 shows that this is indeed the case, and thus the charge neutrality argument appears to be valid.

When below-band-gap radiation is used, denoted by $h\nu_2$ in figure 11, the effect of the Schottky junction is negligible because of the increased penetration depth at this wavelength; however, the p^{++}/p interface and the p/p^+ interface must now be taken into account. In this case the polarity of the observed photovoltage due to the built-in field of the p^{++}/p interface is reversed, since electrons will be

swept into the bulk and holes will be swept into the metal. The voltage pulse shape from this interface will tend to follow the laser pulse, since the carriers are generated only 1 μm from the metal/p^{++} interface. Since the absorption depth for $h\nu_2$ is fairly deep (see fig. 8 and 11), the built-in potential of the p/p^{+} interface also contributes to the observed photovoltaic response at these wavelengths. For this junction, the signal polarity will be the same as that produced by the metal/p^{++} interface, with one primary exception. Since the generated carriers are now 20 μm from the collecting metal contact, a significant broadening of the PV pulse shape would be expected. Since the hole mobility in SiC is on the order of 40 $cm^2/V\text{-}s$, this corresponds to a carrier drift time of ≈1 μs (assuming that a built-in field of 100 mV is dropped across the 20-μm epi-layer). Inspection of the 430-nm waveform at $X = 0.0$ mm in figure 6 shows that this explanation is in qualitative agreement with the experiment; the long decay time is on the order of a microsecond.

The high-speed response can best be summed up as follows: since a significant response was measured for photon energies well below the 6H-SiC band-gap energy, one must conclude that the semiconductor contains many impurity centers. These centers obviously permit efficient carrier generation to occur, and the lifetimes of photoinduced carriers that are related to these impurity centers are extremely short. It must be noted that, unlike that of Si, the free carrier concentration of SiC may be much less than 40 percent of the actual doping concentration [17]. Therefore, the fast behavior may well be caused by the increased ionization of acceptors (here Al for p-type doping), since an increase in majority carriers (i.e., holes) is caused by the optical input. Upon removal of the optical excitation, equilibrium is re-established on picosecond time scales. This is shown by the hole capture time constant of the ionized acceptors, which is given by

$$\tau_c = [N_A v_{th} \sigma_c]^{-1} , \qquad (1)$$

where N_A is the doping concentration, v_{th} is the thermal velocity, and σ_c is the capture cross section. Assuming $N_A = 10^{17}\ cm^{-3}$, $v_{th} = 10^7$ cm/s, and $\sigma_c = 10^{-13}\ cm^2$, then $\tau_c = 10^{-11}$ s, which indicates that picosecond behavior is possible. Therefore a fast response time can be expected, assuming that below-band-gap absorption is mediated by ionized impurities within the 6H-SiC material. The longer PV response corresponds to direct electron-hole recombination, which has been measured for these devices to be on the order of nanoseconds [18]. Thus, the response at 450 nm is most likely a superposition of these two effects. It is interesting that the devices respond to photon energies that are so much lower than E_g.

4. SiC Photoconductive Switch Experiments

Since the dark resistance of both switch types was less than 20 Ω, a low-impedance circuit was used for the photoconductivity measurements. The circuit consisted of a simple dc bias, charging resistor, and load, as shown in figure 12. A carbon-filled resistor was used to minimize unwanted stray inductance. The load resistance indicated is actually the oscilloscope input impedance, which was ac coupled to improve the measurement sensitivity.

A UV dye (Coumarin 440) was pumped with a Laser Science, Inc., N_2 laser (model VSL-337ND) so that the laser wavelength could be tuned around the absorption edge of 6H-SiC. The band-gap energy of this material is 3 eV, which corresponds to a wavelength of 414 nm. I used the N_2 laser output to assess the switch behavior well above band gap. The N_2 laser output energy was ≈200 μJ, with a pulse width of 7.7 ns and a 3-Hz repetition rate. The dye output energy was ≈10 μJ, with the same pulse width and repetition rate.

The measured PC response of a 10-μm-gap lateral PC switch is shown in figure 13 as a function of bias voltage. The calculated on-state resistance was typically 8 Ω. Note that the dark resistance was reduced by 50 percent when the PC switch was illuminated by the laser.

For the vertical devices, similar results were observed, with two exceptions. First, since the switching gap is the substrate itself, a polarity change in the PV response with respect to the beam position across the gridded electrode was not expected or observed. Second, since the vertical switch dark resistance was approximately half the

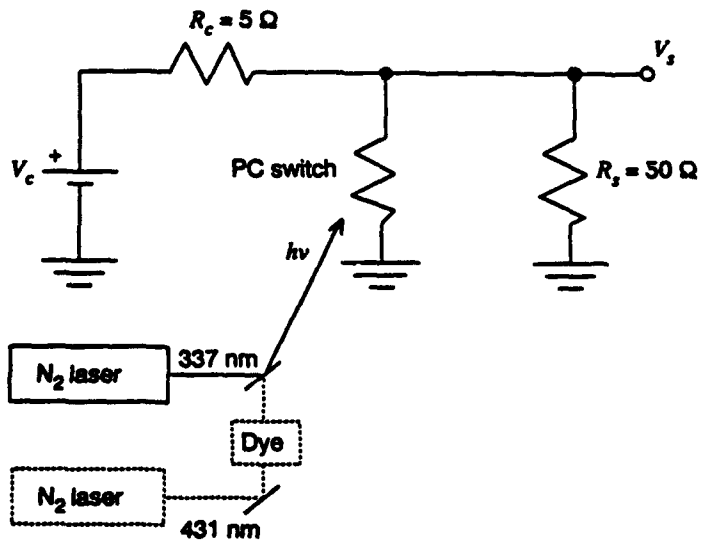

Figure 12. PC response experimental setup showing electrical circuit, optical components, and switch (lateral or vertical) position. R_s is scope impedance.

lateral switch dark resistance, considerable device heating occurred for high bias values. Also, the vertical switches were placed on an insulating surface and were therefore poorly heat sinked. As a consequence, for a device static power dissipation exceeding 11 W, the vertical switch grew to be so hot that it glowed until the switch mount failed. The device was remounted and found to be still operational. The PC switch response is shown in figure 14. R_{on} was 1.9, 2.2, and 1.3 Ω for V_c = 5, 10, and 15 V, respectively.

These effects were observed in a vertical switch with laser radiation that was well above the band-gap energy of 6H-SiC. I then pumped some UV and violet dyes with the N_2 laser so that I could measure the switch response for radiation just above and below the band-gap energy. The band-gap energy of 6H-SiC corresponds to a wavelength of ≈414 nm, and the dyes were chosen to be near this wavelength. The switches responded as anticipated: smaller PC voltages were observed for photon energies well below the band-gap edge,

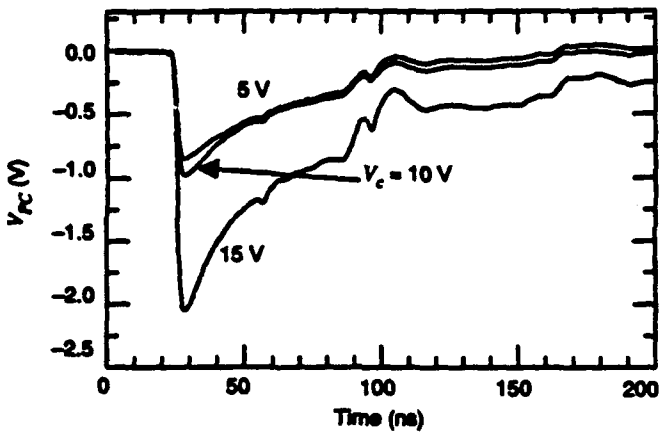

Figure 13. PC response of a 10-μm lateral 6H-SiC switch as a function of circuit bias. Laser parameters are identical to those indicated in figure 12. λ = 337 nm.

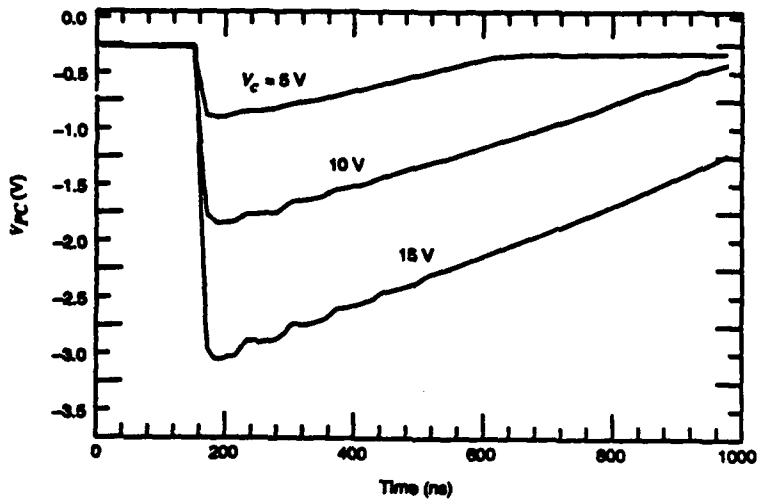

Figure 14. Vertical PC switch response versus circuit bias. Laser parameters are identical to those of figure 12. λ = 337 nm.

with values comparable to those in figure 13 observed for photon energies at and above the absorption edge. The vertical switch efficiency, η, is defined as the ratio of the switched-out voltage pulse amplitude, V_o, to the supply voltage, V_c. With 337-nm radiation and a bias of 5 V, the vertical SiC switch η was 32 percent, and an increasing efficiency was observed for increasing switch bias.

Figure 15 shows the data used to determine the bulk carrier lifetime with below-band-gap (λ = 431 nm) radiation. The *p*-type 6H-SiC displayed a double-exponential PC carrier lifetime decay behavior, which was observed with the lateral switches as well. As indicated in the figure, a fast decay of ≈200 ns was observed. Not completely shown in the figure is the measured slower decay of ≈800 μs. At λ = 337 nm, the fast decay was ≈330 ns, followed by a slower decay of ≈590 μs. In comparison, the surface lifetime measured with the 10-μm lateral switch (fig. 13) was ≈40 ns.

Two distinct carrier decay times, as shown in figures 13 and 15, were measured in 3C-SiC by Okumura et al [4]. I believe that their explanation for the 3C-SiC behavior is also valid for these experimental results in 6H-SiC, namely that the fast component is due to direct electron-hole recombination, while the long decay time is caused by the re-emission of carriers from traps that reside within the energy band gap. I plan further experiments to investigate this hypothesis.

The corresponding carrier lifetime at the switch surface is ≈40 ns. The value of surface lifetime quoted is, however, an estimate, since figure 13 shows a slight variation in this value with applied voltage. The applied voltage also results in an increase in the switch temperature, which may account for this change. Carrier transport effects, such as carrier sweep-out, may also account for this behavior.

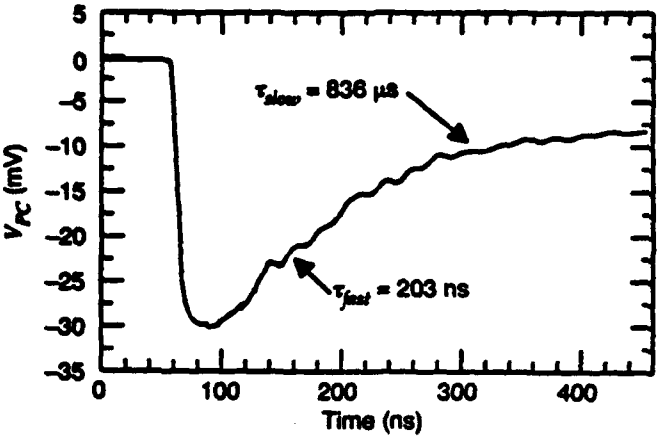

Figure 15. PC carrier recombination lifetime measured with vertical PC switch. V_c = 10 V, λ = 431 nm. Double-exponential decay times, τ_{fast} and τ_{slow}, indicated.

5. Summary

The measurement of efficient photoconductive switching in *p*-type 6H-SiC switches was limited by the low dark resistivity of the material. With higher resistivity substrates, the switching efficiency should improve dramatically, although the value measured with the vertical switch (η = 32 percent) was not for the optimum circuit. The encouraging observation that the vertical 6H-SiC devices can operate at high temperatures obviously has implications for pulsed-power applications. The ability to fabricate large photoconducting devices for high-voltage applications is still, however, uncertain, since we could not hold off large voltages with these devices ($R_{dark} \approx$ 2 Ω). It is important to note that with the vertical structure, substantial photoconductivity was observed at 337 nm, even though this corresponds to a photon energy that is well above the 6H-SiC bandgap energy. We believe that carrier diffusion and drift are responsible for this observed behavior.

This successful measurement of a significant photovoltaic effect in 6H-SiC, even with the observation of ohmic contact behavior in the dark state, indicates that efficient UV photodetection at high temperatures is possible. The very fast carrier decay times ($\tau_{decay} \approx$ 10 ns) observed during these experiments indicate that the UV detection may also be high speed.

The identification of several deep-level electronic impurities may eventually lead to higher resistivity 6H-SiC materials, with the ultimate goal of semi-insulating behavior being achieved. Once this can be accomplished, 6H-SiC will then be suitable for both ultra-fast and high-power PC switching applications, and, in particular, the optoelectronic attenuator scheme [19] can be implemented with SiC for a thermal dissipation much improved over either GaAs or silicon.

Acknowledgement

The author wishes to thank Pak S. Cho, Julius Goldhar, and Chi H. Lee of the University of Maryland, for their invaluable technical assistance during this research project. John W. Palmour of Cree Research, Inc., Durham, NC, is also acknowledged for providing the PC switches for investigation. The High Power Microwave Technology Management Office (HPM-TMO) is gratefully acknowledged for providing the financial support for this work.

References

1. P. A. Glasow, "6H-SiC Studies and Developments at the Corporate Research Laboratory of Siemens AG and the Institute for Applied Physics of the University in Erlangen (FRG)," from *Amorphous and Crystalline Silicon Carbide and Related Materials*, Springer-Verlag Proceedings in Physics, 34, pp 13–33 (1988).

2. J. A. Powell and L. G. Matus, "Recent Developments in SiC (USA)," from *Amorphous and Crystalline Silicon Carbide and Related Materials*, Springer-Verlag Proceedings in Physics, 34, pp 2–12 (1988).

3. S. E. Saddow, P. S. Cho, J. Goldhar, J. Palmour, and C. H. Lee, "Photoconductive Measurements on P-Type 6H-SiC," *SPIE-OE/LASE '93: Optically Activated Switching*, conference proceedings, 1873-33, Los Angeles, CA (January 1993); S. E. Saddow, P. S. Cho, J. Goldhar, J. Palmour, and C. H. Lee, "P-Type 6H-SiC Photoconductive Switches," 20th IEEE International Conference on Plasma Science (*ICOPS '93*), Vancouver, BC, Canada (June 1993); and S. E. Saddow, P. S. Cho, J. Goldhar, J. Palmour, and C. H. Lee, "High-Speed Photovoltaic Response of P-Type 6H-SiC," *Ninth Annual IEEE Sarnoff Symposium* Proceedings, Princeton, NJ (26 March 1993).

4. H. Okumura, K. Endo, S. Misawa, E. Sakuma, and S. Yoshida, "Studies on Carrier Lifetime and Deep Levels in CVD-Grown 3C-SiC," from *Amorphous and Crystalline Silicon Carbide and Related Materials II*, Springer-Verlag Proceedings in Physics, 43, pp 94–99 (1989).

5. M. S. Mazzola, S. E. Saddow, P. Neudeck, V. K. Lakdawala, and S. We, "Observation of the D-Center in CVD-Grown *p-n* Diodes," *Appl. Phys. Lett.* 64, 20 (16 May 1994).

6. P. A. Ivanov and V. E. Chelenokov, "Recent Developments in SiC Single-Crystal Electronics," *Semicond. Sci. Technol.* 7, 863–880 (review article) (1992).

7. M. Bhatnagar and B. J. Baliga, "Comparison of 6H-SiC, 3C-SiC, and Si for Power Devices," *IEEE Trans. Electron Devices* 40 (3), 645–655 (March 1993).

8. V. I. Gavrilenko, A. V. Postnikov, N. I. Klyui, and V. G. Litovchenko, "Energy Band Structure and Optical Properties of Wurtzite-Structure Silicon Carbide Crystals," *Phys. Status Solidi (b)* 162, 447 (1990).

9. V. B. Shields, K. Fekade, and M. G. Spencer, "Near-Equilibrium Growth of Thick High Quality Beta-SiC by Sublimation," *Appl. Phys. Lett.* 62 (16), 1919–1921 (1993).

10. R. F. Davis, G. Kelner, M. Shur, J. W. Palmour, and J. A. Edmond, "Thin Film Deposition and Microelectronic and Optoelectronic Device Fabrication and Characterization in Monocrystalline Alpha and Beta Silicon Carbide," *Proc. IEEE* 79 (5), 677–701 (May 1991).

11. R. J. Trew, J.-B. Yan, and P. M. Mock, "The Potential of Diamond and SiC Electronic Devices for Microwave and Millimeter-Wave Power Applications," *Proc. IEEE* 79 (5), 598–620 (May 1991).

12. J. W. Palmour, R. F. Davis, P. Astell-Burt, and P. B. Blackborow, "Effects of Cathode Materials and Gas Species on the Surface Characteristics of Dry Etched Monocrystalline Beta-SiC Thin Films," *Ceramic Trans.* 2, 491–500 (1989).

13. J. Crofron, P. A. Barnes, J. R. Williams, and J. A. Edmond, "Contact Resistance Measurements on *P*-Type 6H-SiC," *Appl. Phys. Lett.* 62 (4), 384–396 (25 January 1993).

14. J. A. Edmond, H. S. Kong, and C. H. Carter, "High Temperature Rectifiers, UV Photodiodes, and Blue LEDs," from *Amorphous and Crystalline Silicon Carbide and Related Materials IV*, Springer-Verlag Proceedings in Physics, 71, pp 344–351 (1992).

15. D. L. Hatten, Y. Cui, W. T. Hill, T. Mikes, and J. Goldhar, "Generation of Intense 10-ps, 193-nm Pulses Using Simple Distributed Feedback Dye Lasers and an ArF* Amplifier," *Appl. Opt.* 31 (33) (20 November 1992).

16. D. M. Brown, E. T. Downey, M. Ghezzo, J. W. Kretchmer, R. J. Saia, Y. S. Liu, J. A. Edmond, G. Gati, J. M. Pimbley, and W. E. Schneider, "SiC UV Photodiodes," *IEEE Trans. Electron Devices* 40 (2), 325–331 (February 1993).

17. J. M. McGarrity, F. B. McLean, W. M. Delancey, J. Palmour, C. Carter, J. Edmond, and R. E. Oakley, "Silicon Carbide JFET Radiation Response," *IEEE Trans. Nucl. Sci.* 39 (2), 1974–1981 (February 1993).

18. S. E. Saddow, P. S. Cho, J. Goldhar, F. B. McLean, J. Palmour, and C. H. Lee, "Lateral and Vertical *P*-Type 6H-SiC Photoconductive Switch Response," International Conference on SiC and Related Materials (*ICSCRM '93*), Conference Digest, Washington, DC (November 1993).

19. S. E. Saddow and C. H. Lee, *An Optoelectronic Attenuator for the High-Speed Control of Microwave Integrated Circuits*, U.S. Army Research Laboratory, ARL-TR-387 (1994).

Distribution

Admnstr
Defns Techl Info Ctr
Attn DTIC-DDA (2 copies)
Cameron Sta Bldg 5
Alexandria VA 22304-6145

Advnsd Rsrch Proj Agcy
Attn DSO B Hui
3701 N Fairfax Dr
Arlington VA 22203

HQ
Dfns Nuc Agcy
Attn RAEE G Baker
6801 Telegraph Rd
Alexandria VA 22310-3398

Ofc of the Secy of Defs
Attn ODDRE/R & AT S Gontarek
The Pentagon
Washington DC 20301

Army Matl Comnd
Attn AMCRD-AR J Aveta
Attn AMCDE-PQI J Kreck
5001 Eisenhower Ave
Alexandria VA 22333-0001

Belvoir Rsrch Dev & Engrg Ctr
Attn STRBE-NA S Schaedel
FT Belvoir VA 22060-5606

HQ, Dept of the Army
Dep Chf of Staf Oprs & Plns
Attn DAMO-FDI LTC R Morton
Room 2C536 The Pentagon
Washington DC 20310-0460

Hdqtr US Army Cmmctn-Elect Cmnd RD&E Ctr Night Vsn & Elect Sensors Directrt
Attn AMSEL-RD-NV-ADS M Kovach
FT Monmouth NJ 07703-5206

Ofc of the Assist Scy of the Army for Rsrch Dev & Acqstn
Attn SARD-TT F Milton Rm 3E479
Attn SARD-TT C Nash Rm 3E479

Ofc of the Assist Secy of the Army for Rsrch Dev & Acqstn (cont'd)
Attn SARD-DOV LTC B Adams Rm 3E411
The Pentagon
Washington DC 20310-0103

US Army ARDEC
Attn SCMAR-FSP-M R T Kinasewitz
Bldg 353N
Picatinny Arsenal NJ 07806-5000

US Army CECOM Intllgnc/Elect Warfare Drctrt
Attn AMSEL-RD-IEW-SPO D Helm
Vint Hill Farm Sta
Warrenton VA 22186-5100

Commandant
US Army Infantry Schl
Attn ATSH-CDM-E K Sines
FT Benning GA 31905-5400

US Army Mis Cmnd
Attn AMSMI-RD-WS-UB D Holder
Redstone Arsenal AL 35898-8000

US Army Prgm Mgr—Firefinder
Attn SFAE-IEW-FF A Dirienzo
FT Monmouth NJ 07703-5305

US Army Sp & Strtgc Dfse Comnd
Attn CSSD-SL-S R Berg
PO Box 1500
Huntsville AL 35807-3801

Commander
US Army TRADOC
Attn ATCD-T J M Gray
FT Monroe VA 23651

Nvl Rsrch Lab
Attn Code 4650 T Wieting
4555 Overlook Avenue SW
Washington DC 20375-5000

Distribution

Sp & Nav Warfare Systs Comnd
Attn SPAWAR 332 J Albertine
2451 Crystal Park
Arlington VA 22245-5200

Air Force Phillips Lab
Attn PL/WSH H Dogliani
Attn PL/WSH M Harrison
Attn PL/WSH S Mason
Attn PL/WSH W Snyder
3550 Aberdeen Ave SE
Albuquerque NM 87109

Depart of the Air Force
Attn AWP W Baker
Attn PL/XPW P Vail
Kirtland NM 87117-6008

Air Force Rome Air Dev Ctr
Attn ERPT T Pesta
Attn RADC J Rooks
Griffiss AFB NY 13441

Commander
Wright Rsrch Dev Ctr
Attn WRDC/ELM T Kemerley
Bldg 620 Area B
Wright Patterson AFB OH 45433-7408

Los Alamos Natl Lab
Attn K Callahan MS H851
Attn R Reinovsky
PO Box 1663
Los Alamos NM 87545

Sandia Natl Lab
Attn Div 1248 L Bacon
Attn Div 1235 J Hoffman
PO Box 5800
Albuquerque NM 87185-5800

Mississippi State Univ
Attn M Mazzola
PO Drawer EE
Mississippi State MS 39762

Univ of Maryland Electrcl Engrg Dept
Attn C H Lee
College Park MD 20742

Ball Systems Engrg Div
Attn J E Vanderstar
2901 Juan Tabo NE
Albuquerque NM 87124

Consultant
Attn V Van Lint
1032 Skylark Dr
La Jolla CA 92037

GE-CRD
Attn M Ghezzo
PO Box 8 Bldg KW RM B1309
Schenectady NY 12301

Jaycor
Attn W Crevier
3944 State Stret Ste 360
Santa Barbara CA 93105

Mssn Rsrch Corp
Attn M Bollen
Attn J McAdoo
8560 Cinderbed Rd
Newington VA 22122

Mssn Rsrch Corp
Attn D P Snowden
7907 Ostron Stet Ste D
San Diego CA 92111

SPARTA Inc
Attn R O'Connor
4901 Corporate Dr Ste 102
Huntsville AL 35805-6201

SRI Intrntl
Attn G August
333 Ravenswood Ave
Menlo Park CA 94025

Distribution

Westinghouse Electr Corp Elect Sys Grp/BWI fcilty
Attn S Patel Mail Stop 3716
PO Box 1693
Baltimore MD 21203

US Army Rsrch Lab
Attn AMSRL-WT
Attn AMSRL-WT-PC A Barrows
Attn AMSRL-WT D Hisley
Attn AMSRL-WT-P I May
Aberdeen Proving Ground MD 21005-5066

US Army Rsrch Lab
Attn AMSRL-CP-PW L Weinberger
Attn AMSRL-CP-PW T White
Attn AMSRL-DD-M J Scully
Attn AMSRL-DD-SE J Sczepanski
Attn AMSRL-OP-SD-TA Mail & Records Mgmt
Attn AMSRL-OP-SD-TL Tech Library (3 copies)
Attn AMSRL-OP-SD-TP Tech Pub
Attn AMSRL-SL-NB J Beilfuss
Attn AMSRL-SL-ND C Glenn
Attn AMSRL-SS J Sattler

US Army Rsrch Lab (cont'd)
Attn AMSRL-SS-SG J McCorkle
Attn AMSRL-WT-L G Roffman
Attn AMSRL-WT-NA H Briskei
Attn AMSRL-WT-NA R A Kehs
Attn AMSRL-WT-NB J Gwaltney
Attn AMSRL-WT-NF C Fazi
Attn AMSRL-WT-NF E Scannell
Attn AMSRL-WT-NF G Tran
Attn AMSRL-WT-NF J Tatum
Attn AMSRL-WT-NF L Jasper
Attn AMSRL-WT-NF M Berry
Attn AMSRL-WT-NF R Kaul
Attn AMSRL-WT-NF R Tan
Attn AMSRL-WT-NF S Kaplan
Attn AMSRL-WT-NF S Saddow (25 copies)
Attn AMSRL-WT-NF T Turner
Attn AMSRL-WT-NG A Bromborsky
Attn AMSRL-WT-NH A Mark
Attn AMSRL-WT-NH G Huttlin
Attn AMSRL-WT-NH J Corrigan
Attn AMSRL-WT-NH L Libelo
Attn AMSRL-WT-NH S Hayes
Attn AMSRL-WT-NH T Bock